Ice buttressing-controlled rock slope failure on a cirque headwall, English Lake District

Paul A. Carling[a, b,] John D. Jansen[c], Teng Su[d, e], Jane Lund Andersen[f], Mads Faurschou Knudsen[f]

[a] Geography and Environmental Science, University of Southampton, Southampton, SO17 1BJ, UK.

[b] Lancaster Environment Centre, Lancaster University, Bailrigg, Lancaster, LA1 4YW, UK.

[c] GFÚ Institute of Geophysics, Czech Academy of Sciences, Prague, Czechia.

[d] University of Chinese Academy of Sciences, Beijing 100049, China.

[e] Laboratory of Water Cycle and Related Land Surface Processes, Institute of Geographical Sciences and Natural Resources Research, Chinese Academy of Sciences, Beijing, 100101, China.

[f] Department of Geoscience, Aarhus University, Aarhus, Denmark.

Corresponding author: Paul A. Carling (p.a.carling@soton.ac.uk)

Key Points

Geometry and mechanics of cirque rock slope failure defined from the local geology

Rock slope failed slowly due to ice buttressing the cirque headwall

Rock slope failure occurred during deglaciation

Abstract

Rock slope failures in the English Lake District have been associated with deglacial processes after the Last Glacial Maximum, but controls and timing of failures remain poorly known. A cirque headwall failure was investigated to determine failure mechanisms and timing. The translated wedge of rock is thin and lies on a steep failure plane, yet the friable strata were not disrupted by downslope movement. Fault lines and a failure surface, defining the wedge, were used as input to a numerical model of rock wedge stability. Various failure scenarios indicated that the slope was unstable and would have failed catastrophically, if not supported by glacial ice in the base of the cirque. The amount of ice required to buttress the slope is insubstantial, indicating likely failure during thinning of the cirque glacier. We propose that, as the ice thinned, the wedge was lowered slowly down the cirque headwall gradually exposing the failure plane. A cosmogenic ^{10}Be surface exposure age of 18.0 ± 1.2 ka from the outer surface of the wedge indicates Late Devensian de-icing of the back wall of the cirque, with a second exposure age from the upper portion of the failure plane yielding 12.0 ± 0.8 ka. The 18.0 ± 1.2 ka date is consistent with a small buttressing ice mass being present in the cirque at the time of regional deglaciation. The exposure age of 12.0 ± 0.8 ka represents a minimum age, as the highly-fractured surface of the failure plane has experienced post-failure mass-wasting. Considering the chronology, it appears unlikely that the cirque was re-occupied by a substantial ice mass during the Younger Dryas Stadial.

Key words:

rock slope failure, Pleistocene glacial cirque, cosmogenic exposure dating, deglaciation, Younger Dryas, English Lake District.

1 Introduction

There are at least 84 known or suspected rock slope failures (RSFs) in the Lake District of NW England that have been associated with the Late Devensian glaciation (Marine Isotope Stage 2: Wilson *et al*., 2004; Jarman and Wilson, 2015a; Wilson & Jarman, 2022). Such RSFs often are termed 'paraglacial' as they "are part of, or influenced by, the transition from glacial conditions to non-glacial conditions" (Ballantyne, 2002; McColl, 2012). However, the relationship between glaciation, deglaciation, and the occurrence of RSFs remains far from resolved. This paper provides a contribution to further understanding of the topic. While a

few highly modified landforms have been identified tentatively as RSFs and related to time periods before the Last Glacial Maximum (LGM; c., 26.5 ka BP to 19 ka BP, Clark et al., 2009) (Jarman and Wilson, 2015b), the majority of Lake District RSFs have been associated with the end of the Dimlington Stadial (see 'Glacial Context') and the final down-wasting of the Late Devensian ice sheet within NW England. At that time, potential RSFs could have been fully supported or partially supported by residual ice masses in topographic lows. Alternatively, some RSFs could have occurred (Wilson, 2005) following the Scottish Readvance (*c*., 19.3 – 18.2 ka; Chiverrell *et al*., 2018) and the Younger Dryas Stadial (12.9 – 11.2 ka; Rasmussen *et al*., 2006). However, only one disintegrated RSF has been dated. In contrast, those that represent steep-slope deformation, or arrested slides, are of unknown age (Jarman and Wilson, 2015b). An arrested hillslope failure occurs when the slipped mass is not evacuated from the source area (Jarman, 2005), but is retained on the slope of the footwall. The role of glacial ice in buttressing rock slopes, and thereby preventing failure (Whalley *et al*., 1983; Holm *et al*., 2004; Cossart *et al*., 2008; Le Roux *et al*., 2009; Allen *et al*., 2010; Hilger *et al*., 2018), is largely speculative (Ballantyne, 2002; Jarman and Wilson, 2015b; Cody *et al*., 2018; Hartmeyer *et al*., 2020) and controversial (McColl *et al*., 2010), as are the mechanics of slope failure in situations where ice-support progressively diminishes (McColl and Davies, 2013; Klimeŝ *et al.,* 2021; Cave and Ballantyne, 2016). The latter two generic issues are the primary focus of this paper.

Glacial erosion can steepen cirque headwalls to the extent that faulted and/or fractured-rock slopes become unstable (Sass, 2005; Moore *et al*., 2009), if not ice-supported. In addition, the way slopes fail can provide insight to whether ice was present during the slope failure. If ice-buttressed failures can be dated, then RSFs provide a source of information on the timing of the final ice retreat. Here, an arrested (*sensu* Jarman, 2005) translational RSF is described, dated, and the likely controls on the failure are defined and modelled. We test the hypothesis that *a steep, faulted, and unstable rock slope has experienced buttressing by glacial ice*. Our study area, which has not been previously identified as a RSF site, is within Great Coum (54.3923° N, 2.6057° W), a small cirque within the southern Shap Fells to the west of the Lune gorge (Fig. 1). A neighbouring cirque is named Little Coum. The Lune gorge (south of Tebay; Fig. 2) separates the southerly extension of the Shap Fells to the west from the Howgill Fells to the east. The site details and glacial context are described below.

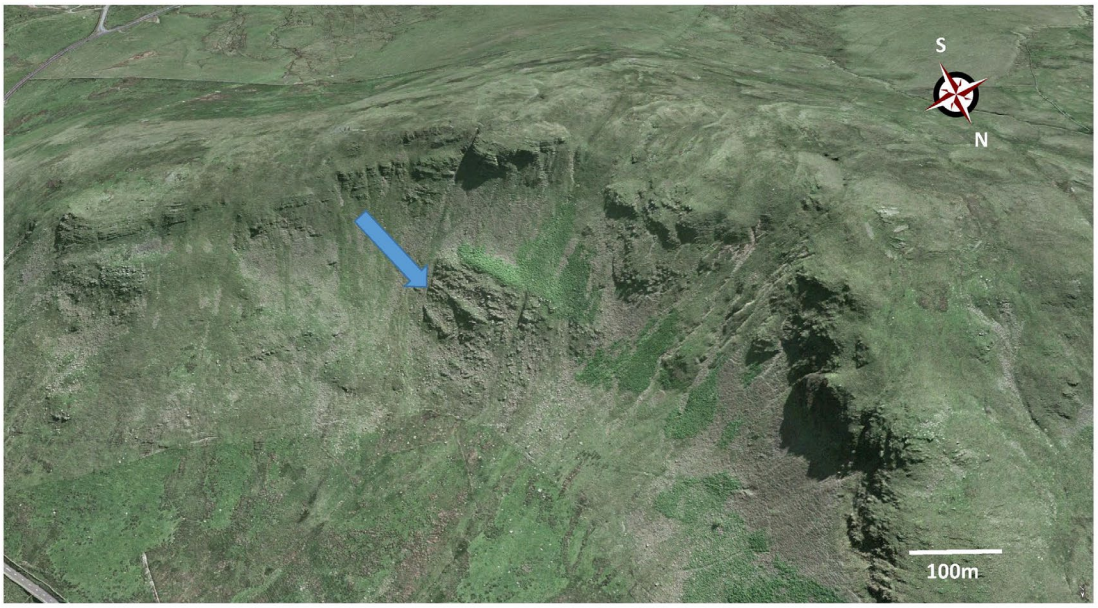

Fig. 1: Oblique aerial view, looking southwestward, into Great Coum (Google Earth image). The RSF is arrowed. The green grassy tread of the RSF (just above the arrow) is in sunlight below the cliffed headwall (in shadow). The breadth of the RSF is between 125m and 180m. Little Coum is just out of view to the right. Base image © Google Earth 2014. Scale bar applies to the middle distance.

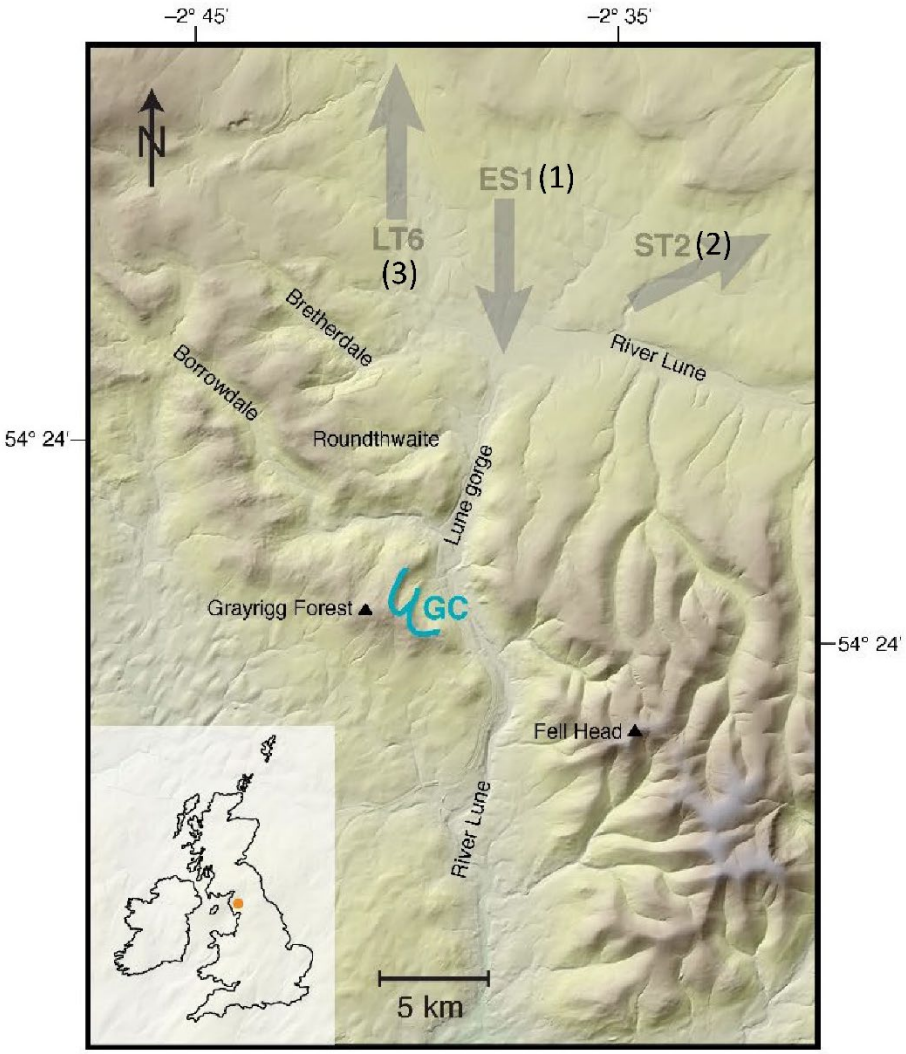

Figure 2: Regional map showing the location of Great Coum (GC) and Little Coum with respect to generalized Dimlington (ES1), (ST2) and (LT6) ice movements (after Livingstone et al., 2010; 2012). Labels (1), (2) and (3) indicate the temporal sequence of ice movements. Locations referred to in the main text are also shown. Inset shows the location of the study area in the context of the British Isles. Base NEXTMap digital elevation topography has a 5 m resolution.

2 Glacial Context

The last period of extensive glaciation in northern Britain occurred during the Dimlington Stadial of the Late Devensian substage of the Pleistocene (~28-15 ka; Rose, 1985; Scourse *et al*., 2009; Chiverrell and Thomas, 2010; Davies *et al*., 2019), equivalent to Stadials 3 and 2 of the North Greenland Ice Core Project (NGRIP) chronology (Lowe *et al*., 2008) and the Marine Isotope Stage 2 (Ehlers and Gibbard, 2013). During the LGM, the Lune gorge and surrounds were covered by several hundred metres of ice. The Lune gorge is ice-sculpted, having a

parabolic bedrock cross-section with truncated valley-side spurs along both the west and the east margins. Great Coum and Little Coum, on the western side of the gorge, are the only recognized cirques in the Lune gorge. These two Lunedale cirques should not be confused with two cirques with the same names in Dentdale (Barr *et al*., 2017). The two conjoined embayments were considered by Marr and Fearnsides (1909) to be a single cirque, but recently have been recorded as separate cirques (Barr *et al*., 2017; Clark *et al*., 2018). Devensian till banks and moraine (entrenched by the River Lune) fill much of the Lune gorge floor and till also occurs in most tributary valleys (Aveline *et al*., 1888; Marr and Fearnsides, 1909; BGS, undated; 2008 a and b).

2.1 Complexity of Devensian glaciation around Great Coum

The context in which the RSF occurred is relevant to the interpretation of the importance of potential ice buttressing and is referred to within the Discussion. Here we provide the setting. Little is known of the glacial history of the Lune gorge area (Carling *et al*., 2023). Nevertheless, prior findings, in the main, have been incorporated in the BRITICE maps of the area (Stokes *et al*., 2018). A complex interplay occurred in the vicinity of the Lune gorge between several upland ice dispersal centres, primarily: the Scottish, Lake District and Howgill ice masses, during the period of maximum ice cover ~ 26–22 ka. All three ice masses interacted in the north whilst the latter two ice masses dominated to the south. After the LGM, as the ice sheets down-wasted and ice flows became increasingly valley-confined, ice emanating from the two cirques would have flowed northwards (Carling *et al*., 2023).

The complexity of regional ice flow was simplified by Livingstone *et al*. (2010; 2012) by using codes to refer to different ice streams (Fig. 2) that occurred in various locations and at differing times; the relevant codes are as follows. In the ES1 phase, early LGM, northern ice penetrated a short distance into the Lune gorge (Harkness, 1870; Goodchild, 1875; 1889; Marr and Fearnside, 1909; Hollingworth, 1931; Moulson, 1966; Letzer, 1978) as far as Carlingill and Great Coum (Fig. 2) but no further. However, Davies *et al*. (2019) demonstrated that, close to the LGM, (ST2 phase; *sensu* Livingstone *et al*., 2010) and during the LT6 phase (Chiverrell *et al*., 2018), ice flowed northwards from the Lune gorge (Fig. 2). On the northern flank of the Howgill Fells, any ST2/LT6 ice flow would have been to the

144 north and east from the Howgill ice dome (Fig. 2) such that the higher summits of the
145 Howgill Fells were not overrun by ice from further north (Gunson, 1966; Stone *et al*., 2010).
146 Rather, the Howgill Fells hosted its own local ice dispersal centre. Prior work failed to
147 determine whether northern ice entered the two Lunedale cirques. Consistent northerly
148 down-wasting ice-flow was established (Hollinsworth, 1931; Rose and Letzer, 1977) from 19
149 ka (Davies *et al*., 2019) with surrounding areas north and south of the Lune gorge being ice
150 free by ~ 19.2 to 16.6 ka (see Carling *et al*., 2023, for a review of regional dates). These dates
151 are broadly consistent with other dates for deglaciation of the central Lake District more
152 widely (Wilson and Lord, 2014) and are indicative of a general ~ 2–3 kyr window for the
153 timing of final Dimlington ice down-wasting within the Lune gorge when the back wall of the
154 Great Coum cirque could have become ice-free. We return to this point in sections 3 and
155 6.2.
156
157 Given that ice may have reoccupied upland terrain in Lake District during the Younger Dryas
158 (Brown *et al*., 2013; Bickerdike *et al*., 2018), in principle, an ice mass may also have occurred
159 in the general vicinity of the Lunedale cirques at this time. However, no evidence for
160 Younger Dryas ice in the Lune gorge has been reported.
161
162 **3 Geological Setting of the cirques**
163
164 The bedrock in the cirques comprises the marine Silurian Coniston Group (Soper, 1999;
165 Soper, 2006), which here consists of fine-grained, blue-grey, sandy siltstone (greywacke) and
166 sandstones in beds from < 1 m to ~ 3 m thick. Most of the thicker beds crop-out within the
167 headwalls of the cirques. The thicker sandstone beds are more competent with fewer
168 fractures, whilst thinner fissile siltstone beds exhibit cleavage and are heavily fractured.
169 Vertical joints are frequent with spacings of a few metres, together with evidence of small-
170 scale bedding deformation and small-scale faulting. Moseley (1968; 1972) considered the
171 considerable complexity of the regional structure and noted folding, steep discontinuous
172 local faulting, joint patterns and the presence of slickenside surfaces in the southern Shap
173 Fells. In the Methods and the Results, this complexity is not considered, as the detail is not
174 pertinent to our study. None-the-less, reference is made to local steep faults, slickenside
175 surfaces and friability where these are relevant, as the rock structure in the vicinity of the

RSF is critical in assessment of slope stability (Bonilla-Sierra *et al*., 2015; Stead and Wolter, 2015). The apparent dips of the local beds range from 0° to 30°, SW into the headwall of Great Coum. However, the apparent 8° plunge of the stratal sequence is towards the NW, such that the true dip is to the WSW with a NW strike (BGS, 2008 a and b). Infrequent, but distinctive 10– 40 mm-thick pale bands of siltstone occur (*e.g.,* Taylor *et al*., 1971, p. 26) in some of the thicker beds, which extend discontinuously over distances of several decametres parallel to the primary bedding. These siltstone bands are significant in that examples (here termed marker horizons) occur in the headwall strata which correlate with similar siltstone bands in the strata of the RSF.

Great Coum is orientated NE, Little Coum is orientated NNE. The orientations of the cirques are influenced by the strike of local paired anticlines (Marr and Fearnside, 1909; BGS, 2008a), and the low-insolation aspects of both sites would have encouraged Devensian snow and ice accumulation and preservation. Great Coum exhibits no distinct lip (i.e., no overdeepening), the ground falls steadily from around 237 m (height above mean sea level, m asl) to the River Lune below (Fig. 3A). Above 300 m the ground rises more steeply to rocky head walls locally near 80° at 360–440 m, giving a height range of around 225 m. Little Coum exhibits a slight lip at around 262 m altitude. Above 400 m the ground rises more steeply to near 80° rocky head walls at 400–440 m, and the ridge crest at 480 m gives a height range of around 220 m (Fig. 3B). First to second-order minor streamlets occupy the lower parts of Great Coum, and Little Coum is drained by the third-order stream, Burnes Gill.

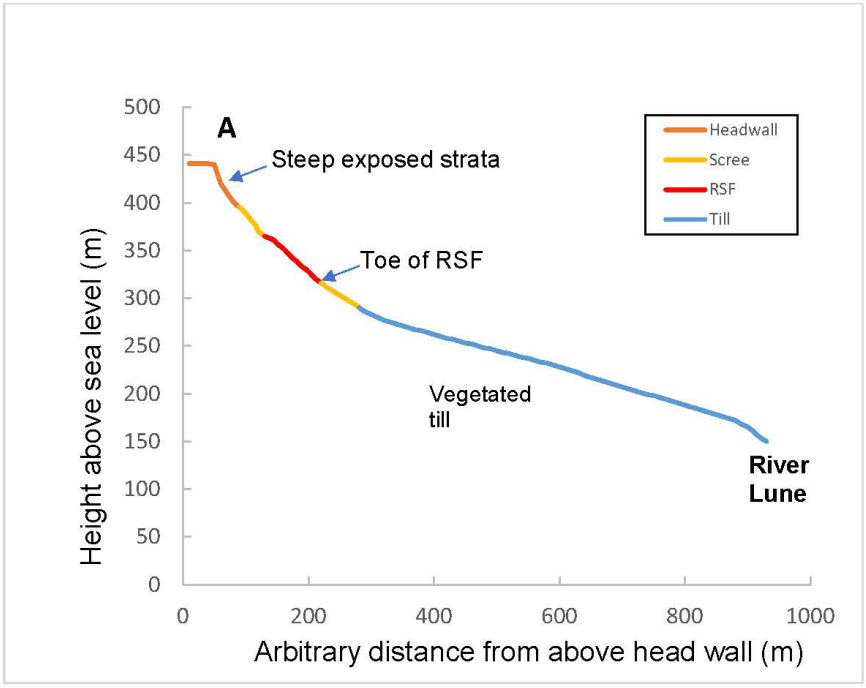

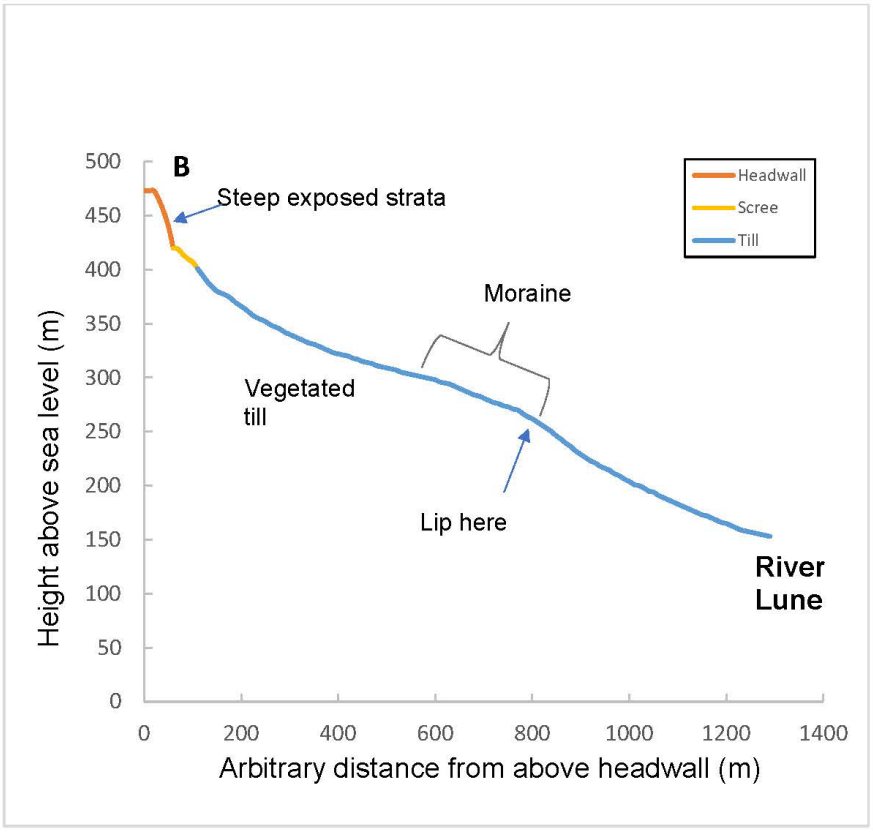

Figure 3: Long profiles along centre of cirque: (A) Great Coum; transect from 54.389978 N; 2.606625 W to 54.396675 N; 2.598278 W; (B) Little Coum; transect from 54.393789 N; 2.615992 W to 54.400117 N; 2.602208 W. Exposed bedrock is indicated in the headwall and in the RSF. Data extracted from Google Earth.

The British Geological Survey (BGS,2008b) map identifies till on the lower slopes of Great Coum and the BGS borehole database contains the records of 24 shallow boreholes ranged along the axis of the Lune gorge over 1.25 km immediately below Great Coum. These borehole logs show that the slopes just below the cirque consist of a thin soil above a 2.5 m thickness of Devensian diamicton, overlying the Silurian Coniston Grit. In Little Coum, hummocky till infills the cirque below 400 m (BGS, 2008b); at lower altitudes, a flatter thin diamicton drapes much of the basin, including a poorly defined curvilinear moraine that terminates at the lip (Fig. 3B). It is not possible to calculate an equilibrium line altitude (ELA) with any certainty based on the upper limit to highest lateral limits to the curvilinear moraine (Porter, 2001), but 300 m asl is a reasonable estimate. Bedrock exposures along Burnes Gill and augering during the current project indicate that this moraine is no more than 6 m thick. The curvilinear moraine has a distinctive, sharp, outer margin along the rocky rounded ridge that separates the two cirques. Within Little Coum, three faint diamicton-covered (possibly ice-recessional) benches occur on the northern slope of the cirque. Thus, although Great Coum lacks any preserved indication of ice retreat, such indicators may exist within Little Coum.

All the deposits described above are significant. In the first instance, substantial till in the Lune gorge below Great Coum has been related to northern ice penetrating the gorge around the LGM (Carling, *et al*., 2023). At that time, the whole region was covered by a thick ice sheet (Merritt *et al*., 2019). However, as down-wasting led to increasing topographic control and valley glaciers predominated, there was likely to be ice flow out of the cirques prior to the near-complete ice retreat that left the diamicton-covered benches. We envisage that around the LGM, thick overriding ice in the vicinity of Great Coum was dictated by regional ice gradients largely independent of the local topography (Carling *et al*., 2023). Post-LGM, ice-discharge from the cirque initially would have remained high but any buttressing effect on the headwall would decline as the ice thinned.

The RSF occurred in Great Coum. The most southerly backwall section of the cirque consists of a steep rocky headwall facing N, whilst to the west a further steep rocky headwall faces NE; a steep grassy slope occurs between these two outcrops. The RSF caused headwall retreat in the vicinity of the present grassy slope, leaving the intact steep rocky sections of

the backwall to either side, but the failure also extends below the north-facing headwall (Fig. 1). Indistinct, small RSFs also occur to the east and west, which are not considered further. Little Coum also contains a steep rocky headwall, but with no evidence of slope failures. The mass of the RSF in Great Coum appears to have descended as a translational near-intact block. Although a near-vertical fracture occurs in the right-hand side of the slipped mass (Fig. 4), in other respects the undisturbed strata within the block readily correlate with strata in the headwall above.

4 Materials and Methods

4.1 Mapping landscape features

The British Geological Survey (BGS, 2008a) records several lineaments in the vicinity of Great Coum that represent small faults or large block joints. Google Earth satellite images (2004, 2009, 2011 and 2014) were used to visually identify these linear landscape features as well as others of relevance (not recorded by the BGS). Lineaments trace topographic discontinuities, stratigraphic offsets, vegetation differences and slickensides, and these forms were checked in the field. Smaller-scale linear features consist of the silt banding marker beds, and numerous minor joints (the latter not mapped). The various points of interest were recorded as single point data in the field using a hand-held Garmin global positioning system (GPS). The strikes of bedding and the direction of faults were recorded as compass bearings whilst the dips of bedding and faults were recorded relative to a horizontal plane using a digital clinometer.

Single point data are precise in planview whereas linear features, between two or more well-determined points, provide the general trend of features such as gullies and faults. GPS coordinates also were used to map the extent of the slumped block. Due to the inaccuracy of hand-held GPS-derived altitudes, the planview GPS coordinates were used to determine the altitude of each point from Google Earth, and these were taken as definitive (error < 4%) after cross-checking with Ordnance Survey 1:50,000 maps (Harley, 1975). Selected topographic profiles were also developed from Google Earth imagery by reading *x*, *y* and *z* coordinates at 10m horizontal spacings along selected planview lines running from the top of the headwall of each cirque, across the free face and the slope below. Finally, a systematic search was made within both cirques for Shap granite or limestone erratics to

check whether northern ice had entered the cirques. Outcrops of both these lithologies occur 10km to the north.

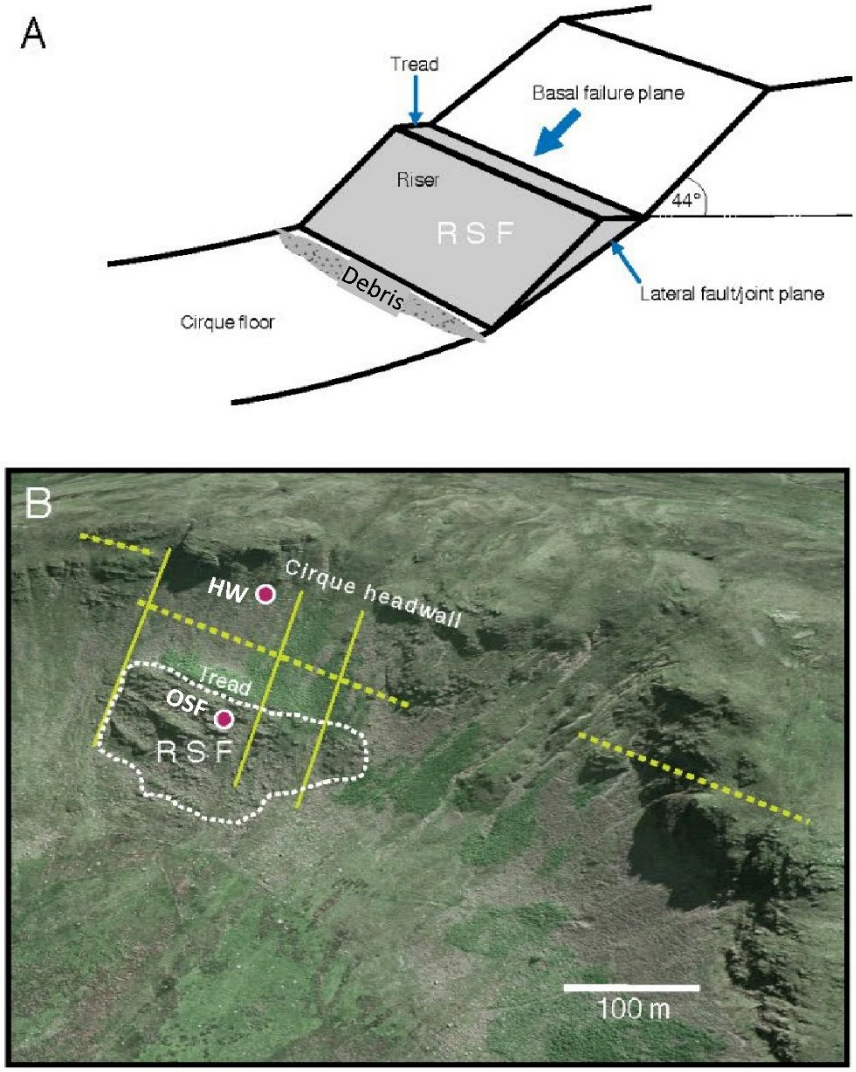

Figure 4: A) Schematic cartoon of a simple wedge failure to indicate the terminology used within the main text. B) Annotated view of Great Coum (compare Fig. 1). The fault-aligned rock slope failure plane (c), above and behind the RSF, is intersected by three major steep fault lines, the outer two of which (X,Y) define the RSF model. The locations of samples (HW and OSF) collected for exposure dating are shown by circled symbols. Base image © Google Earth 2014. Scale bar applies to the middle distance.

We refer the reader to Figure 4A for an explanation of the RSF terminology used here, although the failure planes bounding the wedge are omitted for clarity. The modern

285 headwall of the cirque locally constitutes the main exposed scarp of the failure plane behind
286 the translational wedge of the RSF. The outer face of the wedge is termed the 'riser' and the
287 near-horizontal head of the wedge is termed the 'tread'.
288
289 **4.2 Rock sampling for surface exposure dating**
290 Terrestrial cosmogenic radionuclides, such as ^{10}Be, are produced and accumulate in minerals
291 within a few metres of Earth's surface due to their exposure to secondary cosmic rays and
292 are lost via erosion and radionuclide decay (Lal, 1991). In our case, two free rock surfaces
293 are recognised (Fig. 4): the riser, being the outer surface of the RSF, and the tread, which
294 forms the top surface of the slipped mass. We set out to determine when the RSF riser was
295 first exposed to cosmic rays as ice receded from the cirque. For reasons of economy, we
296 collected one sample from the riser to compare the exposure age with the timing of
297 regional deglaciation. A ~15 kg intact block of bedrock (sample OSF) was collected from the
298 outer 10 cm-thick surface of the riser (Fig. 4B); a prominent thick undisrupted stratum close
299 to the top of the RSF mass, which was ice?-smoothed (Fig. S3). Our sampling strategy was
300 restricted by the ease of access and by the nature of the bedrock surfaces. The smooth
301 bedrock surface of the riser we sampled suggests minimal loss of rock mass due to surface
302 fragmentation or spalling since the RSF occurred. A second 15 kg bedrock block (sample
303 HW) was collected from the failure plane of the transverse fault line (Fig. S3) just below the
304 cirque headwall (Fig. 4B) with an aim to determine the timing of the failure. The sampled
305 bedrock failure plane was observed to be densely fractured, suggesting some loss of
306 material from the surface since its exposure. Surface erosion affects the abundance of
307 cosmogenic nuclides and the estimated exposure age; an issue we address in the Discussion
308 (and Supplementary Materials). Samples were cut from *in situ* bedrock surfaces using a
309 powered rock saw, their altitude, bearing, tilt, and topographic shielding were recorded.
310 Topographic shielding is significant for both samples; details are given in Fig. S1
311 (Supplementary Materials).
312
313 Our approach entails three important assumptions about the last glaciation. First, we
314 assume that the cirque headwall experienced at least 2 m of bedrock glacial erosion, which
315 removed the nuclide inventory produced during preceding ice-free periods; and second, that
316 ice burial depth at the position of the OSF sample was at least 20 m and therefore sufficient

317 to effectively halt nuclide production and third, that this cover persisted until failure. These
318 assumptions mean that sample OSF began accumulating ^{10}Be only from the time that the
319 down-wasting ice exposed the surface to cosmic rays. In contrast, sample HW remained
320 deeply shielded (> 5 m) within the cirque headwall until the RSF exposed the failure plane
321 to cosmic rays.

322

323 ### 4.3 Cosmogenic nuclide analysis

324 The two bedrock samples were prepared for cosmogenic ^{10}Be analysis at the Aarhus
325 University Cosmogenic Nuclide Laboratory, Aarhus, Denmark, following standard laboratory
326 procedures as described in Andersen *et al*. (2020). The ^{10}Be/^{9}Be ratios were analysed at the
327 accelerator mass spectrometer at AARAMS, Aarhus, Denmark. A summary of the
328 cosmogenic nuclide analyses is given in Table 1 and further details are found within
329 Supplementary Materials.

330

331 **Table 1.** Summary of the cosmogenic nuclide analyses. ^{10}Be concentrations in quartz
332 normalized to the "07KNSTD" standardization by Nishiizumi *et al*. (2007), and exposure ages
333 calculated using LSDn scaling (Lifton *et al*., 2014) and global calibration dataset (Borchers *et*
334 *al*., 2016) via http://hess.ess.washington.edu v3.0.2. The analytical uncertainty includes AMS
335 error on measured ratios incl. standard uncertainty of 1.1. %, Be carrier concentration, and
336 processing blank propagation (<1.2 %). The total uncertainty also includes production scaling
337 and calibration uncertainties. Rock density was assumed as 2.7 g cm^3.

338

Sample ID	Latitude	Longitude	Elevation (m.a.s.l.)	Topo shielding correction	Sample thickness (cm)	^{10}Be (at g^{-1})	Uncert (at g^{-1})	^{10}Be age (ka)	Analytic uncert (kyr)	Total uncert (kyr)
HW	54.3907	–2.6065	415	0.74	1	57499	1975	12.0	0.4	0.8
OSF	54.3917	–2.6064	348	0.58	1	63969	2017	18.0	0.6	1.2

339

340 ### 4.4 Rock slope failure modelling

341 The RSF was modelled using *Swedge* version 6.0 (2018), a specialised rock-slope stability
342 software package, which can analyse a five-sided block (pentahedron) as a translational
343 wedge-failure—whereby a rock mass slides along a persistent basal plane of failure
344 bounded on each side by a fault or joint plane (Hoek and Bray, 1981; Rocscience Inc., 2018).
345 Either, or both, laterally bounding faults can act as additional slide planes, depending on

346 the geometry of the problem (Fig. 4A). In our case, two surfaces are not confined by
347 neighbouring bedrock: the outer surface of the RSF, the riser, and the top surface of the
348 slipped mass, the tread (Fig. 4). As well as varying the geometry of the failure and the
349 roughness of the failure planes, *Swedge* has options to consider the influence of: (i) a
350 tension crack at the back of the failure (not shown in Fig. 4A); (ii) water in the failure planes;
351 and (iii) the effect of any restraining normal stress that may counter the propensity to slide.
352 In engineering applications, restraining normal stress is conventionally realized using steel
353 rock bolts, or stone and concrete structures applied to the face of the riser, especially near
354 the toe. In contrast, here the issue is whether an ice mass in the cirque can buttress a slope
355 that is otherwise unstable, as is explored below. In glaciated mountain environments,
356 permafrost (and ice segregation) can penetrate bedrock to a depth of several metres
357 (Andersen *et al*., 2015). Ice-filled fissures tend to be stable at temperatures below –2°C,
358 which gives rise to the concept of 'ice-cemented' fractures (Ballantyne, 2018).
359 Consequently, the possibility that permafrost stabilized the RSF failure planes is considered
360 in section 5.3.
361
362 *Swedge* was implemented adopting the Mohr-Coulomb failure criterion (*e.g.,* Jaeger and
363 Cook, 1979) pertaining to the limit equilibrium stability of a three-dimensional rock mass
364 using field data (Table 2). Further details are provided in the Supplementary Materials and
365 within the Results. Stability is defined in terms of a factor of safety (F) where $F > 1$ indicates
366 a stable slope and $F < 1$, a failed slope. $F = 1$ represents a critical state. In general terms,
367 the factor of safety is defined as the ratio of the forces resisting motion to the driving forces.
368 Driving forces include the mass of the wedge accelerated through gravity and water
369 pressure; the latter applied normal to each wetted plane. Resisting forces arise from the
370 shear strength of the wedge sliding planes. Any ice load on the wedge is considered only as
371 a weight force contribution to the normal stress. Thus, active support due to the load of any
372 glacial ice (or firn) on the riser is included in the analysis as in Equation 1; where T_n is the
373 normal component and T_s is the shear component of the force applied to the riser. Active
374 support is assumed to act in such a manner as to decrease the driving force in the factor of
375 safety calculation:
376

$$F = \frac{resisting\ force + T_n \tan\phi}{driving\ force - T_S} \qquad (1)$$

Unless parameter values are known exactly, a single deterministic RSF model cannot be resolved using Equation 1. In view of the uncertainty, in our field case, related to the exact relationship between fault plane alignments and dips, a variety of potential failure

Table 2. Parameter values for RSF as determined in the field and as explored within the three model scenarios.

	Riser Angle °	Tread Angle °	Riser length (m)	Riser Bearing °	Width of tread (m)	Breadth of RSF (m)	Failure Plane Dip °	Failure Plane Bearing	Failed volume (m^3)	Fault X Dip orientation °N	Fault Y Dip orientation °N	Fault X bearing °N	Fault Y Bearing °N	Fault X Dip °	Fault Y Dip °	Tension crack
Field	53	1	70	24	15	179	44	11	Est: 68288	291	298	21	28	unknown	unknown	unknown
Model 1	53	1	75	24	15	182	44	24	68333	201	208	21	28	80	72	none
Model 2	53	1	75	24	15	182	44	24	67792	90	90	21	28	71	71	none
Model 3	53	1	110	17	15	125	44	11-14	68739	111	62	21	28	90	62	present

scenarios must be considered. To narrow the number of models, we used preliminary trials of our field-derived parameter values as input, varying both strength and slope and geometry parameters. Then, consideration of a range of fault plane dips allowed us to exclude geometrically impossible configurations and those geometries that did not resemble the geometry of the RSF. In this manner, we devised three model scenarios that represent the RSF in terms of shape and mass. More than 10,000 simulations were performed for each scenario, varying parameter values systematically (typically ± 10%) to isolate the most probable model for each case. The uncertainty and probability analyses were conducted using the dedicated approaches built into the *Swedge* platform, selecting normal distributions to describe the possible range of parameter values; for example, ± 10^o of dips measured in the field. Finally, the buttressing effect of any glacial ice against the potential RSF is considered by applying an external load evenly across the area of the riser to counter any propensity for failure.

5.0 Results

5.1 The rock slope failure

The positions of the pale silt marker beds, located in the headwall and within the RSF, indicate the RSF has moved downslope by about 110 m (*H*) vertically and up to 192m (*L*)

horizontally. The width of the tread is about 15 m; the breadth of the slide is between 125 and 180 m and the vertical extent of the main slipped intact mass along the outer face (the riser) is about 70 m. Assuming the displaced block is a triangular wedge thinning towards the toe (Fig. 4), the volume of the intact slip is ~ 68,250 m^3. Below the main slip there is an area of disintegrated rubble which could increase the length of the riser, potentially adding ~ 3 % (~ 2300 m^3) to our volume estimate (Table S1 Supplementary Materials). The value of *H*/L is sometimes considered a mobility ratio, whereby large values of *L* for relatively small vertical displacement (*H*) can indicate unimpeded rapid descent and a long runout. Given the volume of the RSF, values of $H/L > 0.6$, as here, indicate no excessive runout (Whittall *et al.*, 2017; Table S1 Supplementary Materials).

The slope of the riser of the RSF mass is currently ~ 30°, that is, is similar to the static angle of repose. This angle may suggest slow downslope movement rather than rapid failure, which tends to produce slope angles much less than the angle of repose. In addition, there was no evidence of hard-rock end-point control at the toe of the slumping block to impede its descent although the toe has rotated outwards (Fig. 4A). The slope of the riser today is less than the slope of the failure plane (44°), which suggests a portion of the intact wedge may be lying above debris derived by over-running some of the disintegrated thin toe of the wedge (Fig. 4A). It is significant that the stratigraphic layers within the main RSF wedge remain intact, with no evident down-slope dilation and little deformation or fracture across the face of the slipped mass. The apparent plunge of the strata (8 to 10° towards the north), *i.e.,* across the face of the RSF, indicates that the western margin of the slip may have descended slightly further downslope than the eastern margin, as the headwall strata plunge 6° to 8° in the same direction. The outer face (Fig. 4B) of the RSF has undergone no evident modification.

As shown in Figure 4B, a distinct fault (BGS, 2008b), normal to the cliff face occurs to the east of the RSF at location X, with undisturbed stratigraphy in the headwall either side. Slickenside structures occur along the basal failure plane (c) that continues across the cliff to the north-west. The fault X is aligned with the south-eastern margin of the RSF (as seen in Fig. 4B), whilst a further fault is evident as a distinct fissure in the RSF, with another fault to

434 the north-west (Y). The easterly dip of these three faults could not be determined accurately
435 although they are steep, consistent with the findings of Moseley (1968; 1972) for the
436 Coniston group in the region (see section 5.3). The basal failure plane defined the back of
437 the RSF, whilst the lateral limits to the RSF model were defined by the two marginal fault
438 lines (X,Y).
439
440 **5.2 Estimation of original angle of the outer slope of the rock surface before failure**
441 To apply the *Swedge* model it is necessary to know the angle of the outer slope of the rock
442 face before failure. From the geometry of the residual RSF mass, with respect to the
443 observed failure plane (Fig. 4B), the RSF can be considered as a translational, plane failure of
444 a pentahedron wedge. Taking a side view, the geometry is triangular (Fig. 4B), so it is
445 possible to calculate the minimum slope of the outer rock face prior to slope failure by
446 repositioning the failed block further up the failure plane. The angle of the failure plane is
447 taken as equal to that of the minimum angle of the slickenside surfaces, 44^{o}, with a bearing
448 of between 6 and 11^{o}. The riser (outer face) of the RSF is 70 m in length and the tread width
449 is 15 m; both lengths could have been slightly larger before fracturing occurred along the
450 basal failure plane and at the toe of the RSF (Fig. 4A). Given the small degree of uncertainty
451 with regard to the configuration of the slope before failure, the length of the failure plane
452 (necessarily longer than the riser of the RSF) was varied systematically at the same time as
453 varying the length of the riser between the measured length of 70 m and 90 m; the latter
454 value includes the small area of disintegrated toe (Fig. 4A). The tread width also is varied
455 between the measured breadth of 15 m and a 'limit' of 20 m to allow for potential
456 disintegration along the failure plane at the back of the tread. Repositioning the RSF upslope
457 in this manner, the slope of the outer face could have been no lower than 53^{o} and if the
458 angle of the failure plane is increased beyond ~ 54^{o}, the resulting lengths of the failure plane
459 and outer face become incompatible with field observations.
460
461 **5.3 The Swedge model of the rock slope failure without ice buttressing**
462 Initial application of the Swedge Model used the field data shown in Table 2. We did not
463 model the stability of the wedge in its present position because the basal friction properties
464 are unknown; whether the toe of the RSF rests on rubble derived from the failure plane, or a

bedrock surface cannot be determined. Given that the present angle of the riser is 30^{O} and the basal failure plane is at an angle of 44^{o} it is assumed that the wedge is now stable (F>>1).

The slope of the riser utilized is that applicable to the rock mass before failure, as determined in the preceding section. The width of the tread and the lateral extent (breadth) of the failed mass are determined from the field data. The summit of the cirque is fairly flat so an outward slope of 1^{o} below horizontal is used for the tread; the model is not sensitive to this parameter. The angle of the failure plane is the minimum value for the slickensides to the south-east of the RSF (which were not disturbed by the slope failure). The model allows for defining the additional effective roughness angle (*r*) on the failure planes by applying a 'waviness' parameter (*w*) that was determined from the range of recorded slickenside values, following Miller (1988). Other parameters were defined from the field data. It was noted above that the dip of the two lateral delimiting faults could not be determined in the field. However, as local faults tend to be steep (Moseley, 1968; 1972) the model was implemented with the values shown in Table 2 and then varied systematically as reported below. Given the geometry of the problem only three modelling scenarios are necessary to explore the uncertainty in a controlled setting:

Model 1: the RSF slides over the basal plane and against Fault Y. The model aligns the compass orientation of the basal failure plane with the orientation of the riser outer face, which assumes a simple downslope slide. The orientation of Faults X and Y with respect to north are as determined from field data. The X and Y fault dips are steep and both dip to the west. Dips and riser length were varied slightly to optimize the failed volume of the RSF to match the field estimate. In this manner, the model is not consistent with the eastern side of the slip having progressed less far down the failure surface than the western side. Factor of Safety: 0.83.

Model 2: the RSF slides along the basal plane and against Fault X. The model aligns the bearing of the failure plane with the bearing of the slickensides to the east of the RSF, as these define the bearing of the basal failure plane that differs from the bearing of the riser face by 13^{o}. The bearings of Faults X and Y are as determined from field data. The fault dips are steep and both dip to the east. Dips and riser

length were varied slightly to optimize the failed volume of the RSF to match the field estimate. In this manner the model is consistent with the eastern side of the slip having progressed less far down the failure surface than the western side. Factor of Safety: 0.86.

Model 3: explores the addition of a tension crack to the back of the RSF. It is not known if a tension crack developed in the actual rock mass before failure, and the properties of the tension crack are determined by the other model attribute values. Including a tension crack, the western side of the RSF extends further down slope than the eastern side, with the lower edge of the model block having a plunge of ~ 10°, equal to the plunge of the RSF strata in the field. The bearing of the basal failure plane is varied between 6° and 14°. Fault dips are steep, 90° and 62° to the east. Dips and riser length were varied slightly to optimize the failed volume of the RSF to match the field estimate. Given this scenario the RSF slides over the basal plane and against Fault Y. Factor of Safety: 0.52 to 0.83 depending on basal plane bearing.

Given that there is unavoidable parameter uncertainty, none of the above models is an exact representation of the RSF, although Model 3 is the closest match (Fig. 5). Yet, it is evident that preserving the dip of the basal plane and solving to retain the mass of the failure, any reasonable combination of data leads to a model of the failed block that resembles that seen in nature and, in each case, the Factor of Safety is less than unity. A sensitivity analysis showed that, for reasonable ranges of parameter values (typically ± 10°; outwith those listed in Table 2), usually the geometry of the potential failure did not match that observed and so could be dismissed. Specifically, in the 10,000 simulations of each model, model parameters could be varied (*e.g.,* by ± 5° in the case of angles), retaining a probability of slope failure of 96 %. In most cases the factor of safety was between 0.74 and 0.94, and higher factors of safety could not be produced without significant distortion the geometry of the RSF. In a very few cases of parameter combinations (4 %), a marginal factor of safety of between 1.07 and 1.22 is achieved. In the latter cases, wetting between 20 and 30 % of the fault planes surface areas, due to percolation of meltwater affecting the water pressure, caused the slope to fail.

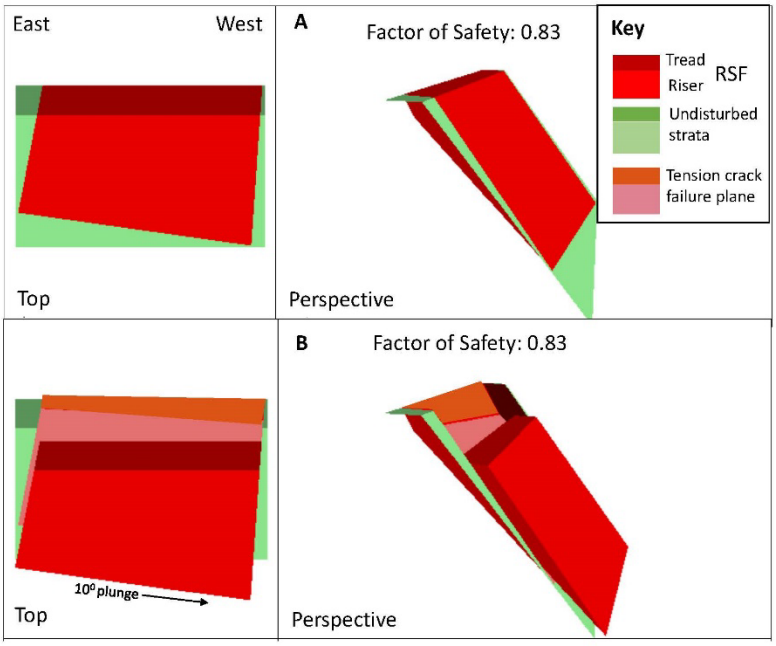

Figure 5: Illustration of Swedge 6.0 Model 3: (A) before failure, and (B) during failure. The basal failure plane orientation is 14º such that the base of the RSF is plunging 10º to the north (right).

As a final consideration it should be noted that in deglaciating mountain regions, RSFs have been related to permafrost degradation and consequent destabilization of ice-filled fractures within the rock mass (Gruber *et al.,* 2004; Gruber and Haeberli, 2007). In the RSF failure model described above, freezing of the failure planes can be considered by simply increasing the friction factors, which can result in the block remaining intact despite the absence of glacial ice buttressing. However, we expect that frozen failure planes did not persist long after glacial down-wasting. Hydrostatic pressure in the failure planes would have been high, and percolation more generally lubricates failure planes (Hasler *et al.,* 2011). In addition, permafrost support for the RSF does not explain the intact stratification of the RSF, as permafrost degradation would have resulted in a rapid RSF. Consequently, permafrost was not considered in any quantitative sense.

5.4 The Swedge model of the rock slope failure with ice buttressing

For the range of simulations reported in the previous section, $F < 1$ in all the 94 % of physically plausible cases and wetting failure planes resulted in a 100 % failure in all 30,000 cases. Hence, the role of ice buttressing of the riser must be considered, as this is the most likely explanation for slope stabilization. There is no information on the dynamic behaviour

551 of ice within the cirque. Consequently, selecting Model 3 above, three contrasting scenarios
552 can be envisaged that might stabilize the slope: (a) ice can be a static load variably
553 distributed around the centroid (Fig. 6A) of the riser; (b) ice can be dynamic, moving towards
554 the riser such that the stress is variably distributed around the centroid of the riser (Fig. 6B);
555 (c) ice can be dynamic, moving away from the riser such that a bergschrund opens between
556 the ice and the slope and the stress is distributed below the centroid of the riser. Broadly
557 consistent results also are found considering Models 1 and 2 (not reported herein).
558
559 Firstly, considering scenario (a), the weight of an ice load is calculated, and the stress is
560 applied evenly across the area of the riser normal (*i.e.,* 90^{o}) to the slope until it is stabilized
561 (for which condition: F = 1.0065; Fig. 6A). Subsequently, considering scenario (ii), the
562 analysis is repeated to ascertain the optimal direction to apply force that minimizes the ice
563 load. In scenario ii, the ice load can be reduced from that in (a) if the force is directed into
564 the slope and slightly upwards by 13^{0} above the horizontal such that for F = 1.0485 (Fig. 6B).
565 In scenario (a), application of 40,659 tonnes of ice is required for a stable slope, which is
566 equivalent to 48,987 m^3, based on a debris-free low ice-density of 830 kg m^{-3} (Colgan and
567 Arenson, 2013). In scenario (b), application of 24,325 tonnes of ice (29,307 m^3) is required
568 for a stable slope. For scenario (c), with a tension crack, the slope will remain stable as long
569 as the total stress applied to the slope is the same as for scenarios (a) or (b). In this study we
570 do not explore in detail how the ice mass and force direction might be distributed across the
571 riser to maintain slope stability as there are multiple permutations. Nonetheless, if the
572 cirque had been filled with ice to the top of the riser, around 166,000 m^3 of ice would be
573 required to fill the volume immediately adjacent to the potential RSF (Fig. 7), which is not
574 compatible with the small ice masses in scenarios (a) and (b) that are required to maintain
575 slope stability. Considering Fig. 7, it is important to recognize that, in any permutation of
576 potential RSF geometry (Table 2), the ice cover required to maintain slope stability is
577 typically less than 29 % (and possible as low as 17 %) of the volume to the top of the riser.
578 This result indicates that the slope would have remained stable as long as there was a
579 sufficiently small degree of ice buttressing due to ice in the cirque contributing a stress
580 normal to the face of the riser—which further implies failure occurred during final
581 deglaciation of the cirque. Note that, although the presence of sufficient ice on the riser
582 alone maintains rock mass stability, it is unlikely that this condition would pertain without

ice present immediately adjacent to the rock wedge. So, Figure 7 shows cirque ice beyond the unstable slope, but only conceptually.

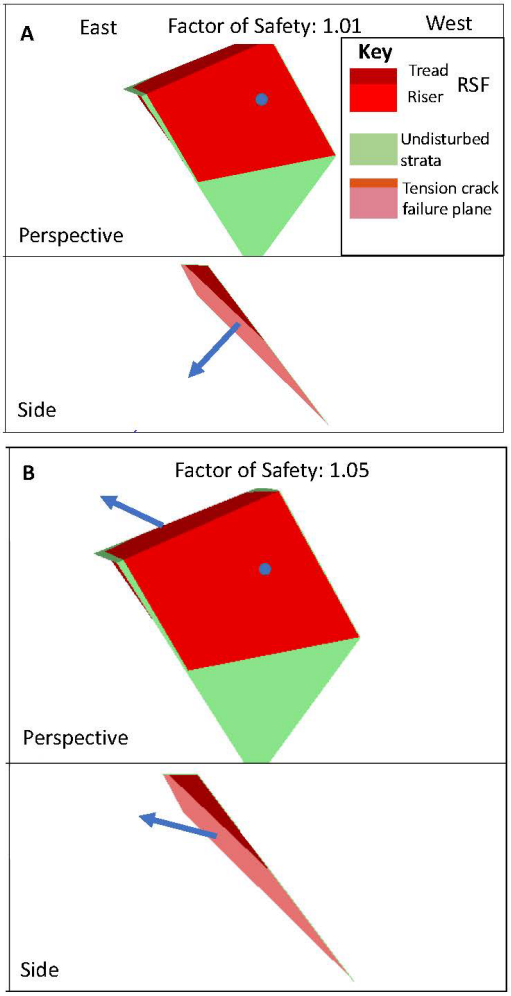

Figure 6: Illustration of the force application required to stabilize the potential RSF: (A) With the force (point and arrow) applied 90° to the slope, the ice load required to stabilize the slope (i.e., F = 1.0055) is 40,967 tonnes; (B) With the force (point and arrow) applied at the optimum angle (13° above horizontal) the ice load required to stabilize the slope (i.e., F = 1.0485) is 28,253 tonnes.

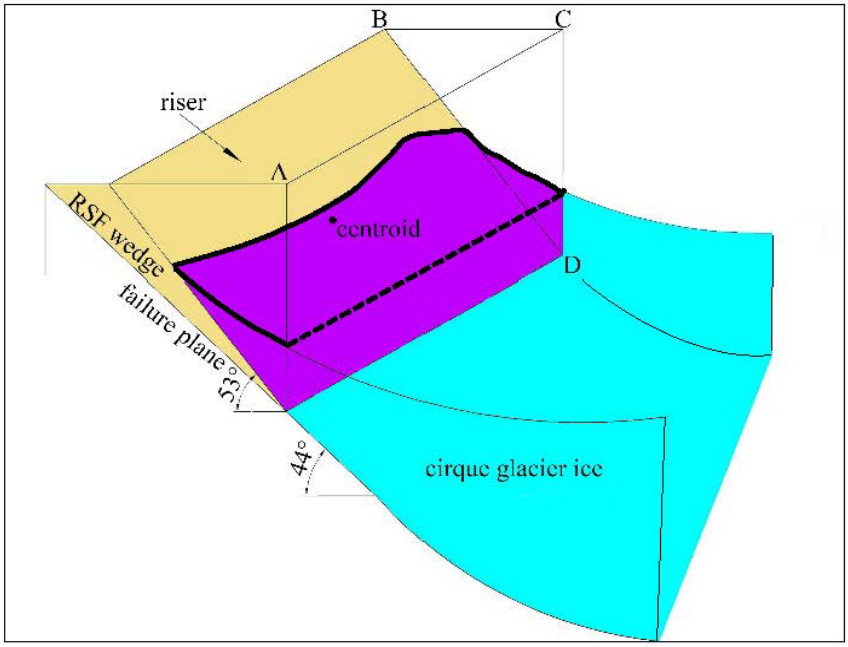

Figure 7: Cartoon depicting the concept of ice buttressing of the potential RSF. The RSF wedge defines the unstable portion of the slope before the rock slope failure. Points A, B, C and D define a potential pentahedral volume that, if filled by ice, would cover the complete face of the riser. A smaller 'pentahedral' volume (purple), with the upper ice surface outlined by a heavy black line, shows that only a small percentage of the potential pentahedral ice volume is required to be ice-filled to provide buttressing sufficient to prevent slope failure. The inner edge of this pentahedral is show as irregular to indicate potential variable ice loading across the riser. Percentages were obtained from the ice volumes required to buttress the slope. Additional ice might be present in the cirque outside of the defined volume, but this ice does not contribute to the stabilizing load directly applied to the riser.

5.5 Exposure ages from the rock slope failure

In both cirques, tills are composed of local lithologies exclusively, and a search for northern-derived erratics confirmed their absence. The absence of erratic lithologies indicates that the cirques were probably finally eroded by locally generated ice masses after the LGM. At the time of the LGM, it is thought that the locations of the cirques were overridden by an ice sheet from the north moving into the northern end of the Lune gorge (Carling *et al*., 2023). Under such thick ice conditions, the back wall of the cirque would have been stable as the volume of ice was much greater than that required for slope stability—shown by either ice-loading Model 3 scenario a or b. After the LGM, the ice volume in the cirque would decrease such that ice-loading also decreased such that the RSF slowly descended as the

loading fell below a critical F-value to sustain the slope. It is this lowering of the RSF that we have attempted to date with cosmogenic nuclides.

The surface exposure age of 18.0 ± 1.2 ka (sample OSF) postdates the timing of maximum ice cover and is consistent with the timing of deglaciation within the broader region (Carling *et al*., 2023) as is considered in the Discussion. As was noted in section 4.2, the outer face of the RSF (the riser) constitutes a smooth surface of intact, undeformed strata, so concordance of the surface exposure age and regional dates is to be expected. Exposure of the RSF riser (sample OSF) predates significantly the exposure age of 12.0 ± 0.8 ka (sample HW) calculated for the RSF basal plane, suggesting a relationship between debuttressing of the riser face and the gradual downward slip of the RSF. The younger age for sample HW is expected, due to the basal failure plane being progressively exposed after the upper portion of the RSF (where sample OSF occurs) was clear of ice cover and the RSF began to move downslope. Also of significance is the fact than the basal failure plane was disrupted by the failure and is friable, as was noted in section 4.2. The loss of only one or two small blocks from the location sampled on the failure plane at any time after failure should result in an age younger than that of the outer face of the RSF (see Supplementary material). Results of the cosmogenic nuclide analyses are summarised in Table 1.

6.0 Discussion

6.1 Modelling the RSF dynamics

The *Swedge* model was applied to the RSF assuming the original slope of the rock face was 53^{o}, with a slide plane angle of 44^{o} and no ice buttressing. The steeper slickenside surfaces observed in the field directly above the RSF could indicate a steeper failure plane than that used in the model, but these values were not used as they may represent strata disturbed by the RSF. In any case, an increase in the failure plane angle, or the initial angle of the rock face, both increase the propensity for failure. The waviness number calculated from field data and applied in the model is low, which increases the propensity for failure. Preliminary trials showed that to stabilize unstable model slopes would require the use of unrealistically large waviness numbers (Miller, 1988) and so the waviness number was not varied in sensitivity analyses. Thus, our results obtained with the *Swedge* model are conservative but

show that the rock face was consistently unstable before failure. The sensitivity analyses accounted for parameter uncertainty and demonstrated that, in most cases, failure would have occurred due to gravity alone. In those few cases where the slope was modelled as marginally stable, moderate water lubrication of the failure surfaces (typically 30% of surfaces) induced slope failure, but the addition of a modest amount of buttressing ice ensured the slope remained stable. As there is no rock obstacle at the toe of the RSF to impede descent, it is reasonable to assume that the slip occurred slowly as the ice decayed. The need for buttressing of the slope to prevent rapid failure indicates that ice support was important (Hilger *et al*., 2018). Thus, our hypothesis '*a steep, faulted, and unstable rock slope has experienced buttressing by glacial ice*' as proposed in the Introduction is corroborated here.

As the amount of Model 3 scenario (a) ice (static load normal to the face) in the cirque decreases, the level of the ice against the riser will fall towards the toe. Thus, the focal point of the force applied to the slope by the ice cover migrates down the riser. As long as the stabilizing load and the direction of the applied force remain sufficient as ice retreats, the detached block will remain stable. However, the load within the cirque is unlikely to be maintained as the ice elevation falls. The applied force also is variable through time and across the riser as ice primarily deforms by internal flow (Hutter, 1983) such that, if any additional pressure were exerted by residual ice adjacent within the Lune gorge, then the ice mass within the cirque would respond accordingly. In particular, the uniaxial compressive strength of ice is low and decreases as ice temperature increases, as will be the case during deglaciation. Although in our model we do not consider the shear stresses associated with the ice in a quantitative sense, brittle fracture of the thin, buttressing ice mass might ultimately occur owing to the constant pressure associated with the mass of the RSF (Bovis, 1982; McColl and Davies, 2013). The presence of a tension crack will redistribute ice load and induce ice segregation (frost-cracking) in the rock (Sanders *et al*., 2012) close to the toe of the rock mass, further reducing the competency. So as the factor of safety falls to close to F = 1, the detached block will slowly move downwards. In the final stages of deglaciation, low-density firn (~400–830 kg m^{-3}) will replace glacier ice (~830–917 kg m^{-3}) offering less support to the RSF.

The RSF failure probably was controlled by distinct intersecting small-scale faults, as has been modelled herein. Within the general area of Great Coum there appears to be two sets of frequent lineaments, one trending to N to NW and the other NE, that intersect to define bedrock blocks. Despite this propensity, the other steep headwalls in these two cirques show no evidence of large-scale instability, although the basal fault plane of the RSF extends (Fig. 4) behind the more western steep buttress in Great Coum, indicating that this slope is also potentially unstable. One fault (BGS, 2008b) and several other lineaments occur roughly normal to this alignment which, in conjunction, might delimit a potential wedge failure on this western buttress. In the specific case modelled, slope failure is highly site-specific depending, in the main, on fault alignments. Steepening of the cirque headwall via glacial erosion may have altered the disposition of the rock mass load, increasing tensile stresses along the fault planes, and promoting the RSF (Ballantyne, 2002). In this respect, the failed slope was pre-conditioned (*sensu* McColl and Davies, 2013) to fail. However, the modelling suggests that unloading likely played a role in controlling the timing of failure and the rate of landslide displacement once initiated. Unloading may simply allow the unsupported preconditioned block to fail, but the stress release accompanying unloading usually is propagated along the fault network resulting in a reduction of internal locking stresses (*i.e.*, the waviness number; Wyrwoll, 1977; Ballantyne, 2002). Other preparatory factors also come into play as the ice load was removed, such as lubrication of the failure planes by meltwater and weathering of the fault planes in general, moving the block closer to F = 1.

6.2 Timing of the RSF

Although there is only one terrestrial cosmogenic date for the riser of the RSF, the surface exposure dating of 18ka (sample OSF) is compatible with the RSF movement during final deglaciation around 19.2 to 16.6 ka (see Carling *et al*., 2023, for a review of regional dates). We interpret the much younger exposure age (~ 12 ka) on the fault plane (sample HW) as the result of postglacial weathering and erosion of the fractured failure plane. In contrast, much of the surface of the riser is relatively intact. Exposure dating necessarily only yields a minimum-limiting age of exposure, except in cases where primary structures (*e.g.*, glacial striations or slickensides) testify to negligible surface erosion. We observed some slickensides locally preserved on the fault plane, but some degree of surface erosion is also indicated by a scattering of talus and a shattered basal failure plane. We provide an estimate

of the magnitude of surface erosion assuming a range of plausible erosion rates in Fig. S2, Supplementary Materials wherein the limitations of having only two cosmogenic samples is addressed.

We note that the locally derived till and absence of northern derived erratics in the cirques suggests that northern ES1 ice did not enter the cirques, despite the presence of abundant (northern) Shap granite erratics in Borrowdale, Roundthwaite valley and Bretherdale just to the north (Carling *et al*., 2023). Thus, buttressing of the slope by ice moving into the cirque from the north can be ruled out. We suggest that the two cirques probably fed valley glaciers associated with diminishing plateau icefields after the LGM (Carling *et al*., 2023), and their final form evolved during deglaciation. The Devensian termination is thought to be a 4–5 kyr period of ice decay just prior to the Last Glacial-Interglacial Transition at ~ 14.7–11.5 ka (Stone *et al*., 2010). During deglaciation, there was unlikely to be sufficient ice in the adjacent Lune gorge to bolster the cirque ice mass.

Regarding slope failures in cirques, Cave and Ballantyne (2016) and Klimeŝ *et al. (*2021) noted that the role of glacial ice support in cirque back wall stability is conditioned by the associated time scales considered. For example, Klimeŝ *et al. (*2021) reported high factors of safety (> 1.95) for potential RSFs beneath glacial ice during the LGM, which is assumed to be the case during full glacial conditions. Ballantyne *et al*. (2014) demonstrated that, following the LGM, the timing of several dated RSFs is not consistent with the probable timing of glacial debuttressing, reporting ages that correspond to deglaciation and well after. In contrast, at Great Coum, the surface exposure age of 18.0 ± 1.2 ka is consistent with regional estimates of the timing of deglaciation (see Carling *et al*., 2023), as was noted above. However, the apparent delay in final exposure of the fault plane, sometime before 12.0 ± 0.8 ka, indicates that a range of exposure ages might be associated with arrested RSFs; indeed, some post-glacial dates may be associated with isostatic controls on slope failure (Ballantyne et al., 2014).

6.3 An ice advance during the Younger Dryas?

An important remaining issue is whether Great Coum could have supported a glacier during the Younger Dryas Stadial. Although the Lake District was essentially ice-free by ~ 14.7 ka,

744 Younger Dryas cooling led to a subset of cirques in northern Britain refilling briefly (Evans,
745 1997). Sissons (1980) argued that many central Lake District cirques were re-occupied by ice
746 during the Younger Dryas, and subsequent studies (reviewed by Brown *et al*., 2011) indicate
747 the presence of cirque glaciers in the central Lake District. However, the lowest Lake District
748 cirque floors are around 320 m asl (Temple, 1965), whereas the basal lip of Little Coum lies
749 at 262 m asl. In this context, Manley (1961) argued that cirques in the Howgill Fells lack
750 evidence for reoccupation during the Younger Dryas because they are too low. Norris and
751 Evans (2017) suggested the ELA in the western Pennines was 580 m asl during the Younger
752 Dryas with the lowest estimate placing the altitude at 445 m asl (Wilson and Clark, 1995).
753 Similarly, in the eastern Lake District, immediately to the north-west of Great Coum, the ELA
754 has been estimated at 400–600 m with 400 m being regarded as distinctly marginal (Wilson
755 and Clark, 1998). Glacial ice only descended to altitudes below 400 m asl where small outlet
756 glaciers were fed from plateau icefields (McDougall, 2013), the extents of which remain
757 controversial (Bickerdike *et al*., 2018). In this respect, Harvey (1997) noted that there was
758 no evidence of ice readvance in the west facing Carlingill, neighbouring Great Coum.
759
760 As the top of the headwall of Great Coum is at 468 m asl, with no extensive plateau above, it
761 seems unlikely that snow supply was sufficient to maintain a Younger Dryas cirque glacier.
762 Others have also noted that Howgill cirques are too low to support Younger Dryas ice but
763 have suggested that the 'fresh' appearance of moraines in some Howgill and western
764 Pennine cirques indicate that Younger Dryas ice was maintained locally by extensive snow-
765 blow (Gunson, 1966; Gunson and Mitchell, 1991; Mitchell, 1996). If correct, this would
766 reduce the ELA locally to as low as 311 m asl (Mitchell, 1996). Mitchell's estimate of ELA is
767 similar to the best estimate for Little Coum (300 m asl), and it is noted by several authorities
768 (Manley, 1961; Temple, 1965; Mitchell, 1996) that the dominant wind direction during the
769 Younger Dryas was from the W and SW, associated with cyclonic disturbances.
770 Nevertheless, we are not convinced by this argument. The extensive SW-facing slopes of
771 Grayrigg Forest and Grayrigg Pike are below the Younger Dryas ELA, so it is unlikely that
772 sufficient blown-snow could have been supplied to support glacial ice within the Great and
773 Little Coums. Our exposure age of 18.0 ± 1.2 ka (sample OSF) denoting ice-free conditions
774 on the outer face of the RSF suggests the cessation of glacial erosion at Great Coum.
775

7.0 Conclusions

We have demonstrated that a RSF in the headwall of a cirque in the Lune gorge occurred as a slow downslope movement of an intact rock mass due to the presence of a supporting glacial ice mass buttressing the failed slope. The estimated RSF timing corresponds with regional deglaciation occurring by at least 18.0 ± 1.2 ka.

Although the case study reported herein supports the role of ice buttressing as a process which may explain arrested RSFs, the vagaries of rock structure from one location to another, coupled with the spatially variable role of isostatic uplift and local meltwater climate (Cave and Ballantyne, 2016) provide strong site-specific controls on the nature and timing of RSFs. Further modelling of RSFs should elucidate the range of conditions associated with incipient failure whilst additional exposure ages for rock surfaces should assist in constraining the timing during which processes such as glacial debuttressing applied.

Code availability

Swedge 6.0 is available from Rocscience Inc., Toronto (www.rocscience.com) for purchase or as a licenced educational package upon application.

Supplement Link

Note to reviewer: A supplement accompanies this manuscript

Author Contribution

PAC devised the project and conducted the fieldwork and the *Swedge 6.0* simulations. TS assisted in fieldwork. PAC and JDJ wrote the manuscript. JLA and MFK conducted the cosmogenic nuclide analysis. All authors contributed to the final presentation.

Competing interests

The authors declare that they have no conflict of interest.

Acknowledgements

Teng Su was supported by the State Scholarship Fund of the China Scholarship Council. Rocscience Inc., Toronto is thanked for supplying *Swedge 6.0* as an educational package. Wishart Mitchell kindly provided a copy of the Gunson (1966) thesis. Mike Cavanagh and the Horned Beef Company are thanked for access permissions to collect rock samples in the cirque. Sam McColl is thanked for commentary on an early version of the manuscript which

contributed to the final presentation. The reviewers, David Jarman and Tim Davies, are thanked for their detailed commentaries on the submission.

Data Availability Statement

The data required as input to *Swedge* version 6.0 (2018) are listed in Table 2. Use of *Swedge* version 6.0 was licensed under an educational agreement with Rocscience Ltd., 2018: www.rocscience.com. The ^{10}Be concentrations and underlying AMS data associated with the ^{10}Be exposure ages are published on GitHub https://github.com/CosmoAarhus/LakeDistrict_CosmoData.

References

Allen, S. K., Cox, S. C., and Owens, I. F., 2010. Rock avalanches and other landslides in the central Southern Alps of New Zealand: a regional study considering possible climate change impacts. *Landslides*, 8, 33-48.

Andersen, J.L., Egholm, D.L., Knudsen, M.F., Jansen, J.D., Nielsen, S.B., 2015. The periglacial engine of mountain erosion – Part 1: Rates of frost cracking and frost creep. *Earth Surface Dynamics*, 3, 447-462.

Andersen, J. L., Egholm, D. L., Olsen, J., Larsen, N. K., and Knudsen, M. F. (2020). Topographical evolution and glaciation history of South Greenland constrained by paired 26Al/10Be nuclides. *Earth and Planetary Science Letters*, 542, 116300.

Aveline, W.T., Hughes, T.M., Strahan, A. 1888. The Geology of the Country around Kendal, Sedbergh, Bowness and Tebay. Memoirs of the Geological Survey, England and Wales, London, 94pp plus 3 Plates.

Ballantyne, C.K. 2002. Paraglacial geomorphology. *Quaternary Science Reviews*, 21, 1935–2017.

Ballantyne, C.K., Periglacial Geomorphology, Wiley, 472pp, 2018.

839
840 Ballantyne, C. K., Wilson, P., Gheorghiu, D. and Rodés, À., 2014. Enhanced rock-slope failure
841 following ice-sheet deglaciation: timing and causes. *Earth Surface Processes and Landforms*,
842 39, 900–913.
843
844 Barr, I.D., Ely, J.C., Spagnolo, M., Clark, C.D., Evans, I.S., Pellicer, X.M., Pellitero, R., Rea, B.R.
845 2017. Climate patterns during former periods of mountain glaciation in Britain and Ireland:
846 Inferences from the cirque record. *Palaeogeography, Palaeoclimatology, Palaeoecology*,
847 485, 466–475.
848
849 BGS (British Geological Survey), http://www.bgs.ac.uk/data/boreholescans/home.html,
850 accessed 2022, undated.
851
852 BGS, 2008a. Geological Survey of England and Wales 1:50,000 geological map series, New
853 Series Sheet 39, Bedrock, Kendal.
854
855 BGS, 2008b. Geological Survey of England and Wales 1:50,000 geological map series, New
856 Series Sheet 39, Bedrock and Superficial Deposits, Kendal.
857
858 Bickerdike, H.L., Ó Cofaigh, C., Evan, D.J.A., Stokes, C.R., 2018. Glacial landsystems, retreat
859 dynamics and controls on Loch Lomond Stadial (Younger Dryas) glaciation in Britain. *Boreas*,
860 47, 202-224.
861
862 Bonilla-Sierra, V., Scholtès, L., Donzé, F.-V., Elmouttie, M. 2015. DEM analysis of rock bridges
863 and the contribution to rock slope stability in the case of translational sliding failures.
864 *International Journal of Rock Mechanics and Mining Sciences*, 80, 67–78.
865
866 Bovis, M.J. 1982. Uphill-facing (antislope) scarps in the Coast Mountains, southwest British
867 Columbia. *Geological Society of America Bulletin*, 93, 804-812.
868
869 Brown, V.H., Evans, D.J.A., Evans, I.S. 2011. The glacial geomorphology and surficial geology
870 of the south-west English Lake District. *Journal of Maps*, 7, 221–243.

Brown, V. H., Evans, D. J. A., Vieli, A. and Evans, I. S. 2013. The Younger Dryas in the English Lake District: reconciling geomorphological evidence with numerical model outputs. *Boreas*, 42, 1022–1042.

Carling, P.A., Su, T., Meshkova, L., 2023. Distribution of Devensian glacial erratics and related evidence elucidate complex ice flow changes across a former ice divide: Northern England. *Proceedings of the Geologists' Association*, 134, 139-165.

Cave, J.A.S. and Ballantyne, C.K., 2016. Catastrophic rock-slope failures in NW Scotland: quantitative analysis and implications, Scottish *Geographical Journal*, 132, 185-209.

Chiverrell , R.C. and Thomas, G.S.P., 2010. Extent and timing of the last glacial maximum (LGM) in Britain and Ireland: a review. *Journal of Quaternary Science*, 25, 535-549.

Chiverrell, R.C., Smedley, R.K., Small, D., Ballantyne, C.K., Burke, M.J., Callard, S.L., Clark, C.D., Duller, G.A.T., Evans, D.J.A., Fabel, D., Van Landeghem, K., Livingstone, S., O Cofaigh, C., Thomas, G.S.P., Roberts, D.H., Saher, M., Scourse, J.D., Wilson, P., 2018. Ice margin oscillations during deglaciation of the northern Irish Sea Basin. *Journal of Quaternary Science*, https://doi.org/10.1002/jqs.3057 (ISSN 0267-8179).

Clark, P.U., Dyke, A.S., Shakun, J.D., Carlson, A.E., Clark, J., Wohlfarth, B., Mitrovica, J.X., Hostetler, S.W., McCabe, M., 2009. The last glacial maximum. *Science*, 325, 710–714.

Clark, C.D., Ely, J.C., Greenwood, S.L., Hughes, A.L.C., Meehan, R., Barr, I.D., Bateman, M.D., Bradwell, T., Doole, J., Evans, D.J.A., Jordan, C.J., Monteys, X., Pellicer, X.M. Sheehy, M., 2018. BRITICE Glacial Map, version 2: a map and GIS database of glacial landforms of the last British–Irish Ice Sheet. *Boreas*, 47, 11–27. https://doi.org/10.1111/bor.12273.

Cody, E., McColl, S., Draebing, D., Cook, S., 2018. Structural control and development of the ice buttressed Mueller rockslide, New Zealand. Geophysical Research Abstract 30, EGU2018-10748, EGU General Assembly 2018.

Colgan, W., Arenson, L.U., 2013. Open-pit glacier ice excavation: brief review. *Journal of Cold Regions Engineering*, 27, 223-243.

Cossart E, Braucher R, Fort M, Bourlès DL, Carcaillet J. 2008. Slope instability in relation to glacial debuttressing in alpine areas (Upper Durance catchment, southeastern France): Evidence from field data and 10Be cosmic ray exposure ages. *Geomorphology*, 95: 3–26.

Davies, B.J., Livingstone, S.J., Roberts, D.H., Evans, D.J.A., Gheorghiu, D.M., Ó Cofaigh, C., 2019. Dynamic ice stream retreat in the central sector of the last British-Irish Ice Sheet. *Quaternary Science Reviews*, 225, 105989.

Ehlers, J., Gibbard, P.L., Overview. In: *Encyclopedia of Quaternary Science, vol. 2*., Elias, S.A. (ed.), Elsevier, Amsterdam, 143-150, 2013.

Evans, I.S., Cirques and moraines of the Helvellyn Range, Cumbria: Grisdale and Ullswater, In: Geomorphology of the Lake District: A Field Guide, edited by J. Boardman, BGRG Spring Field Meeting, 16-18 May 1997, BGRG, pp. 63-87, 1997.

Goodchild, J.G., 1875. The glacial phenomena of the Eden valley and the western part of the Yorkshire Dales District. *Quarterly Journal of the Geological Society*, 31, 55-99.

Goodchild, J.G., 1889. An outline of the geological history of the Eden valley or Edenside. *Proceedings of the Geological Association*, 2, 258-284.

Gruber, S., Hoezle, M. and Haeberli, W., 2004. Permafrost thaw and destabilization of Alpine rockwalls in the hot summer of 2003. *Geophysical Research Letters*, 31, L13504.

Gruber, S. and Haeberli, W., 2007. Permafrost in steep bedrock slopes and its temperature-related destabilization following climate change. *Journal of Geophysical Research*, 112, F02S18.

Gunson, A.R., Some aspects of the Lateglacial Period in the Western Pennines area. Unpublished M.A. thesis, University of Lancaster, 134pp, 1966.

Gunson, A.R., Mitchell, W.A., Combe Scar, In: Western Pennines: Field Guide, W.A. Mitchell (ed.), Quaternary Research Association, London, pp 104- 110, 1991.

Harkness, R., 1870. On the distribution of Wastdale-Crag blocks, “Shap-granite boulders” in Westmorland. *Quarterly Journal of the Geological Society*, 26, 517-528.

Harley, J.B., 1975. Chapter 11 The accuracy of Ordnance Survey maps, In: Ordnance Survey Maps a descriptive manual, HMSO, London.

Hartmeyer, I., Delleske, R., Keuschnig, M., Krautblatter, M., Lang, A., Schrott, L., Otto, J.-C., 2020. Current glacier recession causes significant rockfall increase: The immediate paraglacial response of deglaciating cirque walls. *Earth Surface Dynamics: Discussions*, https://doi.org/10.5194/esurf-2020-8

Harvey A.M., Fluvial geomorphology of north-west England. In: Gregory K.J. (ed) Fluvial Geomorphology of Great Britain. The Geological Conservation Review Series. Springer, Dordrecht, 173-200, 1997.

Hasler, A., Gruber, S., Font, M. and Dubois, A., 2011. Advective heat transport in frozen rock clefts: conceptual model, laboratory experiments and numerical simulation. *Permafrost and Periglacial Processes*, 22, 378–389.

Hilger,P., Hermanns, R.L., Gosse, J.C., Jacobs, B., Etzelmüller, B., Krautblatter, M., 2018. Multiple rock-slope failures from Mannen in Romsdal Valley, western Norway, revealed from Quaternary geological mapping and 10Be exposure dating. *The Holocene*, 28, 1841–1854.

Hoek, E.T., Bray, J.W., Rock Slope Engineering. 3rd ed. Institute of Mining and Metallurgy, London, 1981.

967 Hollingsworth, S.E. 1931. Glaciation of western Edenside and the adjoining areas and the
968 drumlins of Edenside and the Solway plain. *Quarterly Journal of the Geological Society*, 87,
969 281-357.
970
971 Holm, K., Bovis, M., and Jakob, M., 2004. The landslide response of alpine basins to post-
972 Little Ice Age glacial 520 thinning and retreat in southwestern British Columbia,
973 *Geomorphology*, 57, 201-216.
974
975 Hutter, K., Theoretical Glaciology: Material Science of Ice and the Mechanics of Glaciers and
976 Ice Sheets, Springer, 1983.
977
978 Jarman, D., 2005. Large rock slope failures in the Highlands of Scotland: Characterisation,
979 causes and spatial distribution. *Engineering Geology*, 83, 161-182.
980
981 Jarman, D., Wilson, P., Clough Head - Threlkeld Knotts: A perplexing RSF complex. In: The
982 Quaternary of the Lake District - Field Guide, McDougall, D.A. and Evans, D.J.A. (eds)
983 Quaternary Research Association, London, 153–173, 2015a.
984
985 Jarman, D., Wilson, P. 2015b. Anomalous terrain at Dove Crags 'cirqueform' and Gasgale Gill
986 asymmetric valley, English Lake District, attributed to large-scale rock slope failure of pre-
987 LGM origins. *Proceedings of the Yorkshire Geological Society*, 60, 243–257.
988
989 Jaeger, J.C., Cook, N.G.W., Fundamentals of Rock Mechanics, 3rd edn. Chapman and Hall,
990 London, 1979.
991
992 Klimeŝ, J., Novotný, J., Rapre, A.C., Balek, J., Pavel Zahradníĉek, J.C., Strozzi, T., Sana, H., Frey,
993 H., René, M., Štěpánek, P., Meitner, J., Junghardt, J., 2021. Paraglacial rock slope stability
994 under changing environmental conditions, Safuna Lakes, Cordillera Blanca Peru. *Frontiers in*
995 *Earth Science*, 9: 607277. doi: 10.3389/feart.2021.607277
996
997 Lal, D. 1991., Cosmic-ray labeling of erosion surfaces: in situ nuclide production rates and
998 erosion models. *Earth and Planetary Science Letters*, 104, 424-439.

Le Roux, O., Schwartz, S., Gamond, J.F., Jongmans, D., Bourles, D., Braucher, R., Mahaney, W., Carcaillet, J., Leanni, L., 2009. CRE dating on the head scarp of a major landslide (Séchilienne, French Alps), age constraints on Holocene kinematics. *Earth and Planetary Science Letters*, 280: 236–245. https://doi.org/10.1016/j.epsl.2009.01.034

Letzer, J.M., The glacial geomorphology of the region bounded by Shap Fells, Stainmore and the Howgill Fells in east Cumbria. Unpublished M.Phil. thesis, University of London, 340pp, 1978.

Lifton, N., Sato, T., and Dunai, T. J. (2014). Scaling in situ cosmogenic nuclide production rates using analytical approximations to atmospheric cosmic-ray fluxes. *Earth and Planetary Science Letters*, *386*, 149-160.

Livingstone, S.J., Evans, D.J.A., Ó Cofaigh, C., 2010. Re-advance of Scottish ice into the Solway Lowlands (Cumbria, UK) during the Main Late Devensian deglaciation. *Quaternary Science Reviews*, 29, 2544-2570.

Livingstone, S.J., Evans, D.J.A., Cofaigh, C. Ó, Davies, B.J., Merritt, J.W., Huddart, D., Mitchell, W.A., Roberts, D.H., Yorke, L., 2012. Glaciodynamics of the central sector of the last British-Irish Ice Sheet in Northern England. *Earth-Science Reviews*, 111, 25–55.

Lowe, J.J., Rasmussen, S.O., Björck, S., Hoek, W.Z., Steffensen, J.P., Walker, M.J.C., Yu, Z.C. and the INTIMATE group. 2008. Synchronisation of palaeoenvironmental events in the North Atlantic region during the Last Termination: a revised protocol recommended by the INTIMATE group. *Quaternary Science Reviews* 27, 6-17.

Manley, G., 1961. The Late-glacial climate of North-West England. *Geological Journal*, 2, 188-215.

Marr, J.E., Fearnsides, W.G., 1909. The Howgill Fells and their topography. *Quarterly Journal of the Geological Society*, 65, 587- 610 plus plates.

McColl, S.T. 2012. Paraglacial rock-slope stability. *Geomorphology*, 153-154, 1-16.

McColl, S.T., Davies, T.R.H., McSaveney, M.J. 2010. Glacier retreat and rock-slope stability: debunking debuttressing. Delegate Papers, Geologically Active, 11th Congress of the International Association for Engineering Geology and the Environment, Auckland, Aotearoa, 5-10 September 2010, Auckland, New Zealand, 467-474.

McColl, S.T., Davies, T.R.H. 2013. Large ice-contact slope movements: glacial buttressing, deformation and erosion. *Earth Surface Processes and Landforms*, 38, 1102-1115.

McDougall, D., 2013. Glaciation style and the geomorphological record: evidence for Younger Dryas glaciers in the eastern Lake District, northwest England. *Quaternary Science Reviews*, 73, 48-58.

Merritt, J.W., Hall, A.M., Gordon, J.E., Connell, E.R., 2019. Late Pleistocene sediments, landforms and events in Scotland: a review of the terrestrial stratigraphic record. *Earth and Environmental Science Transactions of the Royal Society of Edinburgh,* 110, 39–91.

Miller, S.M., Modelling shear strength at low normal stresses for enhanced rock slope engineering, In: *Proceedings of the 39th Highway Geology Symposium,* Park City, Utah, August 17-19, pp 346-356, 1988.

Mitchell, W. A., 1996. Significance of snowblow in the generation of Loch Lomond Stadial (Younger Dryas) glaciers in the western Pennines, northern England. *Journal of Quaternary Science,* 11**,** 233 - 248.

Moore, J. R., Sanders, J. W., Dietrich, W. E., and Glaser, S. D., 2009. Influence of rock mass strength on the erosion rate of alpine cliffs. *Earth Surface Processes and Landforms,* 34, 1339-1352.

Moseley, F., 1968. Joints and other structures in the Silurian rocks of the southern Shap Fells, Westmorland. *Geological Journal*, 6, 79-96.

Moseley F., 1972. A tectonic history of N.W. England. *Quarterly Journal of the Geological Society of London*, 128, 561-598.

Moulson, J.R., Some Aspects of the Geomorphology of the Lune Basin. Unpublished M.A. thesis, University of Manchester, 1966.

Norris, S.L., Evans, D.J.A., High Cup Plain – a Younger Dryas palaeoglacier. In: Evans D.J.A. (ed.), The Quaternary Landscape History of Teesdale and the North Pennines – Field Guide. Quaternary Research Association, London, pp. 231-236, 2017.

Porter, S.C. 2001. Snowline depression in the tropics during the Last Glaciation. *Quaternary Science Reviews*, 20, 1067-1091.

Rasmussen, S. O., Andersen, K. K., Svensson, A. M., Steffensen, J. P., Vinther, B. M., Clausen, H. B., Siggaard-Andersen, M.-L.; Johnsen, S. J., Larsen, L. B.; Dahl-Jensen, D., Bigler, M., 2006. A new Greenland ice core chronology for the last glacial termination. *Journal of Geophysical Research*, 111 (D6): D06102.

Rocscience Ltd., SWEDGE-Probabilistic analysis of the geometry and stability of surface wedges. Toronto, Canada; www.rocscience.com, 2018.

Rose, J., Letzer, J.M., 1977. Superimposed drumlins. *Journal of Glaciology*, 18, 471-480.

Rose, J., 1985. The Dimlington Stadial/Dimlington Chronozone: a proposal for naming the main glacial episode of the Late Devensian in Britain. *Boreas* 14, 225-230.

Sanders, J.W., Cuffey, K.M., Moore, J.R., MacGregor, K.R., Kavanaugh, J.L., 2012. Periglacial weathering and headwall erosion in cirque glacier bergschrunds. *Geology*, 40, 779-782.

1094 Sass, O., 2005. Spatial patterns of rockfall intensity in the northern Alps. *Zeitschrift für*
1095 *Geomorphologie*, 138, 51-65.
1096
1097 Scourse, J.D., Haapaniemi, A.I., Colmenero-Hidalgo, E., Peck, V.L., Hall, I.R., Austin, W.E.N.,
1098 Knutz, P.C. and Zahn, R., 2009. Growth, dynamics and deglaciation of the last British-Irish ice
1099 sheet: the deep-sea ice-rafted detritus record. *Quaternary Science Reviews*, 28, 3066-3084.
1100
1101 Sissons, J.B., 1980. The Loch Lomond Advance in the Lake District, northern England.
1102 *Transactions of the Royal Society of Edinburgh: Earth Sciences*, 71, 13-27.
1103
1104 Soper, N.J., The Windermere Supergroup of 1:25,000 sheets NY50 and NY60. Southern Shap
1105 Fells and Northern Howgill Fells, Cumbria. British Geological Survey Technical Report
1106 WA/99/35. 18pp plus 8 figures, 1999.
1107
1108 Soper, N J., Notes on the Windermere supergroup of the country between Kendal and the
1109 River Lune (1: 25 000-scale sheets SD59 and SD69 west). British Geological Survey Internal
1110 Report, IR/06/081. 15pp, 2006.
1111
1112 Stead, D., Wolter, A., 2015. A critical review of rock slope failure mechanisms: the
1113 importance of structural geology. *Journal of Structural Geology*, 74, 1-23.
1114
1115 Stone, P., Millward, D., Young, B., Merritt, J. W., Clarke, S. M., McCormac, M., Lawrence, D. J.
1116 D., Main Late Devensian glaciation of north-west England, In: British Regional Geology:
1117 Northern England. Fifth edition. British Geological Survey, Keyworth, Nottingham,
1118 http://earthwise.bgs.ac.uk/index.php/British regional geology: Northern England, 2010.
1119
1120 Taylor, B.J., Burgess, I.C., Land, D.H., Mills, D.A.C., Smith, D.B., Warren, P.T., Northern
1121 England: British Regional Geology, Fourth Edition, London, HMSO, 125pp, 1971.
1122
1123 Temple, P.H., 1965. Some aspects of cirque distribution in the west-central Lake District,
1124 northern England. *Geografiska Annaler*, 47A, 185-193.
1125

Whalley, W. B., Douglas, G. R., Jonnson, A., 1983. The magnitude and frequency of large rockslides in Iceland in the postglacial. *Geografiska Annaler*, 65A, 99–110.

Whittall, J., Eberhardt, E., McDougall, S., 2017. Runout analysis and mobility observations for large open pit slope failures. *Canadian Geotechnical Journal*, 54, 373-291.

Wilson, P. 2005. Paraglacial rock-slope failures in Wasdale, western Lake District, England: morphology, styles and significance. *Proceedings of the Geologists' Association*, 116, 349–361.

Wilson, P., Clark, R. 1995. Landforms associated with a Loch Lomond Stadial glacier at Cronkley Scar, Teesdale, northern Pennines. *Proceedings of the Yorkshire Geological Society*, 50, 277-283.

Wilson, P., Clark, R., 1998. Characteristics and implications of some Loch Lomond Stadial moraine ridges and later landforms, eastern Lake District, northern England. *Geological Journal*, 33, 73-87.Wilson, P., Clark, R. and Smith, A. 2004. Rock-slope failures in the Lake District: A preliminary report. *Proceedings of the Cumberland Geological Society*, 7, 13–36.

Wilson, P., Lord, T.**,** 2014. Towards a robust deglacial chronology for the northwest England sector of the last British-Irish Ice Sheet, *North West Geography*, 14, 1-11.

Wilson, P., Jarman, D., 2022. Rock slope failure in the Lake District, NW England: an overview, *Geografiska Annaler: Series A, Physical Geography*, 104:3, 201-225, DOI: 10.1080/04353676.2022.2120261

Wyrwoll, K-H., 1977. Causes of rock-slope failure in a cold area: Labrador-Ungava. *Geological Society of America Reviews in Engineering Geology*, 3, 59–67.

1159

1160

1161

1162

1163

1164